CONF-891214--9

Hypervelocity Impact Calculations Using CTH: Case Studies

SAND--89-0598C

DE90 002891

Timothy G. Trucano
J. Michael McGlaun
Solid Dynamics Department
Sandia National Laboratories
Albuquerque, NM 87185

Abstract

In this paper, we discuss the use of the CTH shock wave physics code in the calculation of hypervelocity impact phenomena. We emphasize unusual features of the code that aid in understanding the sensitivity of hypervelocity impact calculations to the numerical methodology. A canonical type of impact problem in which a debris cloud is generated and stagnates against a secondary structure is analyzed. We then provide examples of the contributions of advection, interface tracking, and equation of state (EOS) algorithms to CTH simulations of this type of impact, and comment on grid resolution issues. A general conclusion is that while grid resolution is the dominant source of error in the impact simulations, issues related to advection, interface tracking, and EOS are of comparable importance. We also present examples of the application of CTH to 3-D impact problems, illustrating the potential of 3-D computation, and the severe demands it places on current generation computing hardware.

---

1 Introduction

In this paper, we discuss the opplication of CTH, a multi-dimensional Eulerian shock wave physics code [1], by discussing its application to hypervelocity impact problems. CTH is heavily used for this and other types of applications. We will not attempt to provide a broad discussion of examples and capabilities. Rather, we choose to focus on certain features of CTH that are of interest in gaining understanding of some of the more delicate issues of numerical impact simulations.

We do this in the context of one *canonical problem* (CP), depicted in Figure 1. A tungsten cylinder ($L = D = 0.7186$ cm, $\rho = 19.3$ g/cc) strikes a tantalum layer at normal incidence and varying velocity. This is an illustration of a "thin target impact", in which a debris cloud is generated, propagates across a void region, and then stagnates against a secondary structure consisting of several materials. Table 1 lists the various materials, their densities, and their thicknesses:

Table 1. Material Densities and Thicknesses.

MATERIAL	DENSITY (G/cc)	THICKNESS (cm)
Tantalum	16.654	0.2
Void	0.0	8.0
Tantalum	16.654	0.8
Plastic	1.866	0.65
Aluminum	2.7	0.3
Void	0.0	0.3
Aluminum	2.7	5.35

A range of velocities is typical of current problems, but we consider only two: $v = 7.0$ km/s and $v = 70.0$ km/s. For the lower velocity and the choice of materials in the CP, the generated debris cloud is primarily solid fragmented matter, while for the upper velocity the debris cloud is primarily vapor. These regimes are the extrema that we expect to find in investigations of hypervelocity impact generated debris, and so are of particular interest in understanding the sensitivity of computational predictions to details of the numerical modeling. Anderson, et al [2] and Holian and Holian [3] give contemporary descriptions of the intricacies of this problem.

The paper is organized as follows. In Section 2, we are concerned with some features of the numerical hydrodynamics algorithms, as illustrated by CTH, that are relevant to computational simulations of the CP, but not directly discussed in either [2] or [3]. These are (1) details of the velocity advection in the CTH second-order advection algorithm, (2) the importance of interface tracking, and (3) the difficulty of computing the motion of sub-grid size fragments.

In Section 3, we concern ourselves with the sensitivity of calculations to equation of state (EOS) descriptions. Here, we emphasize an unusual consideration, namely, the inclusion of the solid/liquid transition in the EOS formulation. We find that even at the higher impact velocity for the CP the presence of the melt transition has a noticeable influence on the computational results.

In Section 4, we briefly illustrate the 3-D capabilities of CTH by presenting the results of a 3-D simulation of the CP. CTH has features that make it very useful for large, 3-D calculations, as discussed in [1]. We emphasize the role of these features here.

In Section 5, we summarize our major points.

2 Hydrodynamic Sensitivities

The overall information that one seeks from a computational simulation of the CP (axisymmetric, 2-D calculation) is illustrated in Figures 2 and 3. The plots show the evolution, propagation, and stagnation of impact debris for the two velocity regimes of interest. The plots depict the density of material via the intensity of the dot distribution. Figure 2, corresponding to the 7.0 km/s impact, shows far less spread of the debris than the 70.0 km/s case in Figure 3. Note that the back of the projectile also remains somewhat more condensed at 7.0 km/s. This results in "penetrating" damage after stagnation, the second void region actually closing in Figure 2d, and a region of spall appearing at the back of the second tantalum layer. In Figure 3d, on the other hand, the effect of the fast, tenuous debris has been to dent (or blow-off) the front of the second layer of tantalum in a non-penetrating fashion. The resolution in these calculations was 75 uniform zones in the radial direction, 200 uniform zones in the axial

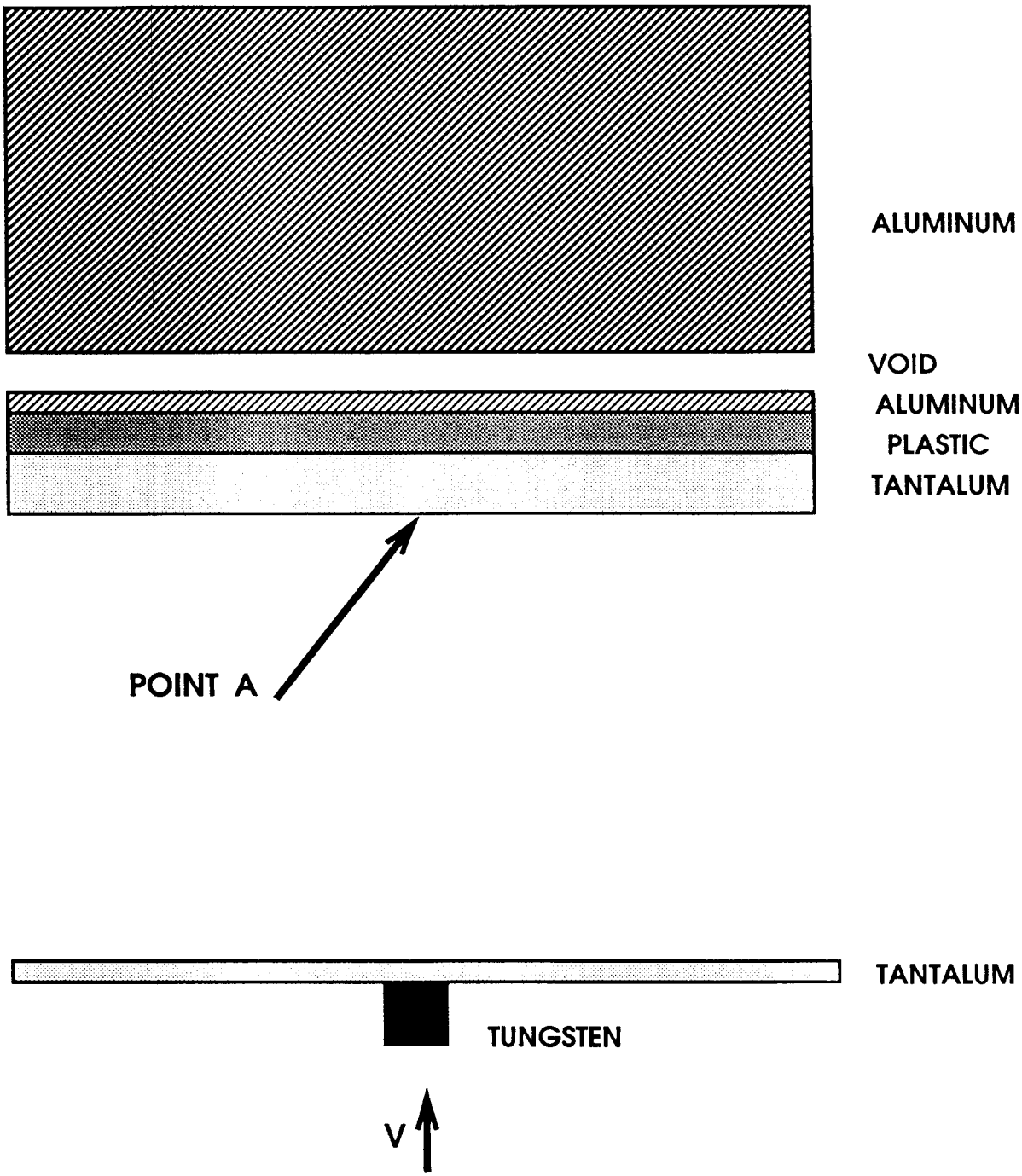

Figure 1: The canonical problem at $t = 0$ μsec.

direction, with $\triangle x = \triangle y = 0.1$ cm.

Point A in Figure 1 is the initial location of a typical Lagrangian tracer particle at which detailed, time-resolved information was recorded. If one views the information in Figures 2 and 3 as somewhat qualitative, Figure 4 presents a quantitative comparison of the two calculations, by plotting pressure vs time at A. Clearly, the pressure loading delivered to the secondary structure by the debris is tremendously different. This is not a surprise. But, while the lower velocity case could actually be compared with experiments, the higher velocity case cannot. The simulated pressure loading is so far removed from what one may confidently compare with experiment that the researcher must concern himself with the intrinsic sensitivities of the calculation to the numerical algorithms.

In this section, we will discuss three of these sensitivities and neglect perhaps the most important one, that of numerical resolution. It is our opinion, and that of other authors ([2], [3], and [4]), that the most dominant hydrodynamic sensitivity in simulating hypervelocity impact problems similar to CP is the resolution of the numerical grid. Problems in which debris is created and propagates through the grid seem to be more sensitive to the resolution than do problems in which thick-target cratering is the dominant phenomenon. (This is not to suggest that cratering calculations can be performed more accurately than problems similar to CP). This, in turn, has suggested to the authors that the order of advection used in the calculations is a "first-order" numerical sensitivity issue for these calculations. This point has also been analyzed in Trucano, *et. al.*, [5] and Asay and Trucano [6] in the context of attempting to match data from carefully controlled shock-vaporization experiments. With this in mind, it is probably wise to view the following as a discussion of "second-order" numerical sensitivities that are, however, at least as important as EOS sensitivities. Additional "second-order" sensitivities that we have not considered include mixed material cell thermodynamics models, the choice of artificial viscosities, and the use of face-centered versus vertex-centered velocities.

2.1 Advection Schemes

CTH allows the user to select one of three different momentum advection options.

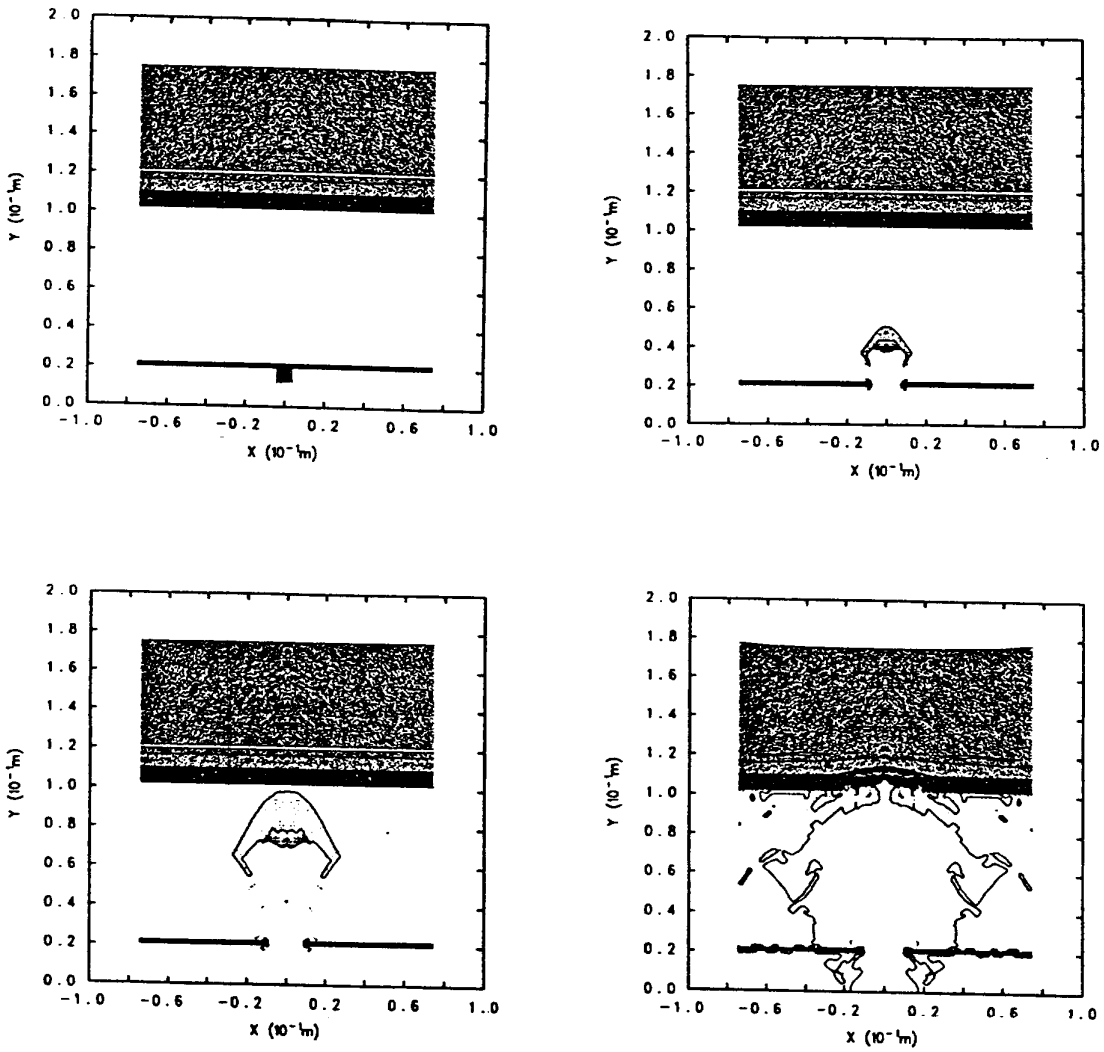

Figure 2: The CP, v = 7.0 km/s, at t = 0.0, 4.0, 10.0, 36.0 μsec after impact. The plots depict density as a function of dot-frequency.

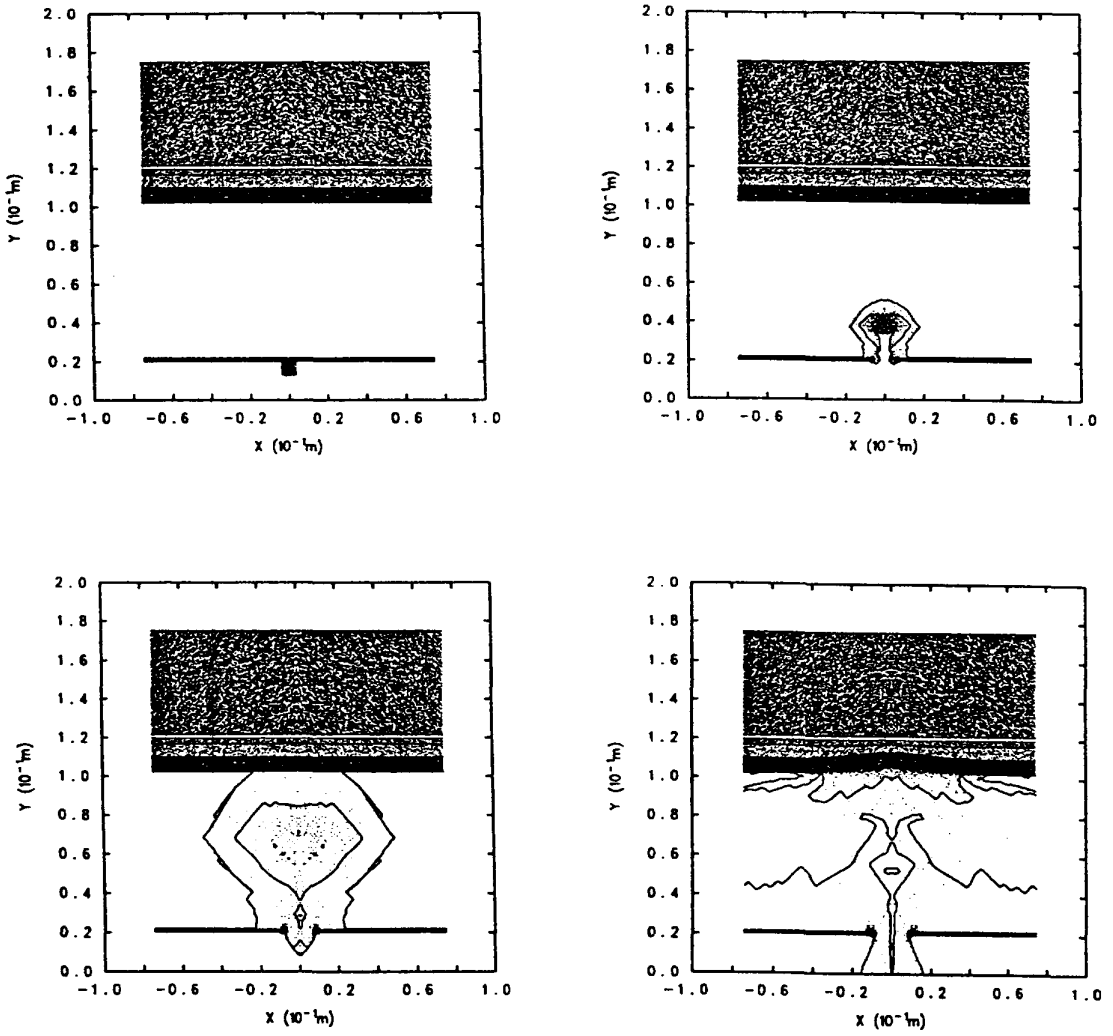

Figure 3: The CP, v = 70.0 km/s, at t = 0.0, 0.4, 1.0, 3.6 μsec after impact. The plots depict density as a function of dot-frequency.

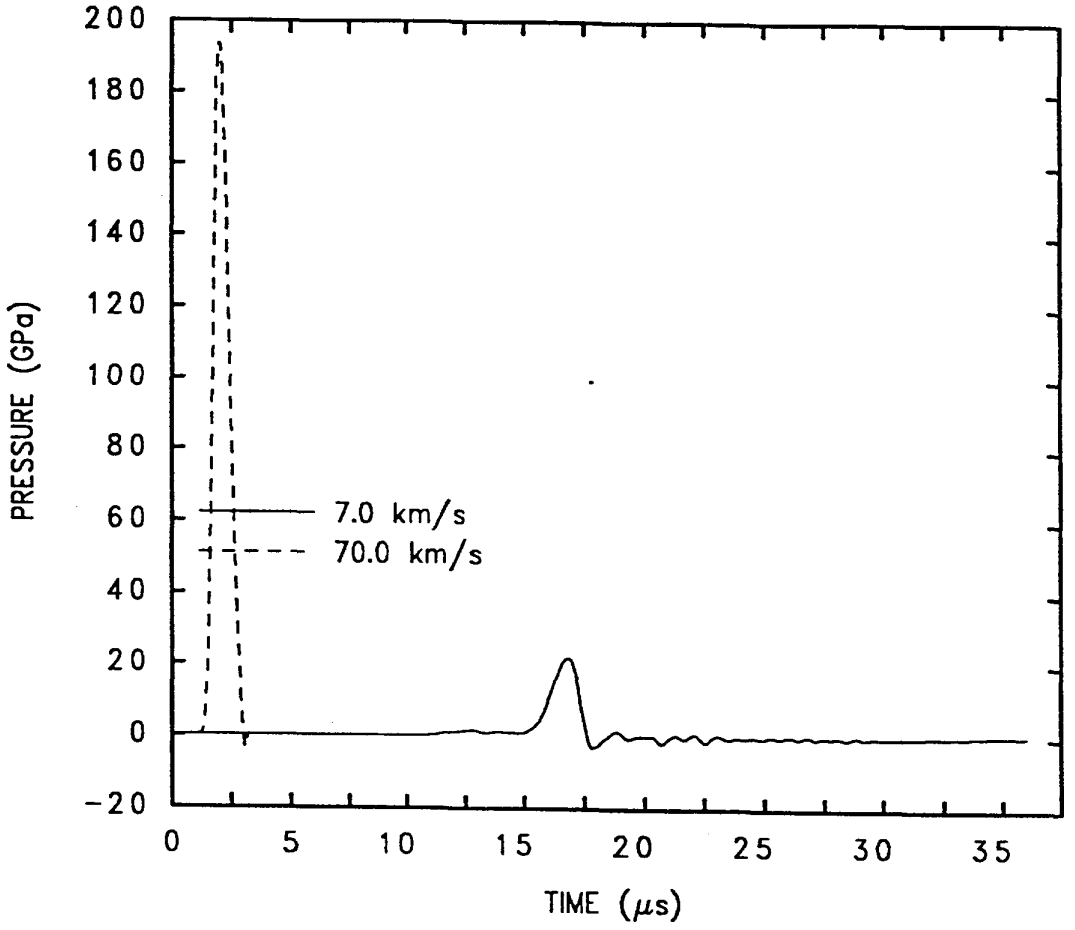

Figure 4: Pressure vs time at A for 7.0 km/s and 70.0 km/s impact velocities.

The underlying second-order scheme in CTH is the van Leer second order monotonic advection scheme that is widely used in modern, multi-dimensional Eulerian hydrocodes (McGlaun, et al, [1]). The difference in the offered schemes lies in the inability to simultaneously conserve both momentum and kinetic energy in a problem during the remapping to the Eulerian grid after the Lagrangian hydrodynamics calculation. In CTH, the user selects a value of the parameter CONV: (1) CONV = 0, in which kinetic energy is conserved and momentum is not; (2) CONV = 1, in which the momentum is conserved, and the kinetic energy discrepancy is discarded; and (3) CONV = 2, in which the momentum is conserved, and the kinetic energy discrepancy is converted to internal energy.

CONV is typically chosen according to the user's experience with particular problems. We have found the CONV = 1 tends to be the best choice for performing hypervelocity impact calculations. More specifically, we have found that CONV = 1 gives the best results when we attempt to compare calculations with normal impact termninal ballistics experiments performed by D. E. Grady [7].

If we compare performance of these schemes on the CP, we obtain the results in Figures 5 and 6. In Figure 5, we have compared the material interfaces of the CP at $t = 10.0$ μsec for $v = 7.0$ km/s and at $t = 0.8$ μsec for $v = 70.0$ km/s, for the three choices of velocity advection. Figure 6 compares pressure vs time at A for both velocities with the three advection schemes.

The interface plots suggest that the distribution of material within the debris cloud is somewhat sensitive to the choice of CONV. In particular, CONV = 2 is clearly allowing the material to expand to a greater degree in the case of $v = 7.0$ km/s, which implies that greater material heating is occuring, something that is likely due to the gain of internal energy from the kinetic energy error. The interface comparisons are somewhat problematic because they don't clearly show the magnitude of the differences, although they are typical of the nature of the experimental data that emerges from terminal ballistics experiments. The pressures at A shown in Figure 6 show huge differences of over 100 % between the lowest and highest peak pressure for $v = 7.0$ km/s, and over 50 % for $v = 70.0$ km/s. These differences in pressure prevail at other locations in the tantalum corresponding to larger values of radius.

The basic point we emphasize is that we can justify the choice of CONV = 1 in terms of experimental comparisons, for $v = 7.0$ km/s. But, how valid is this choice for very high velocity? The fact remains that the "best" solution to the problem of errors in the momentum or kinetic energy conservation may be a combination of the approaches selected by adjusting the CONV parameter, or it may be an entirely different method, such as implementing a higher resolution advection scheme. It may also be highly sensitive to the nature of the problem.

2.2 Interface Tracking

The role of interface tracking is probably equally as important as the order of the advection scheme in certain calculations. The choice of good interface tracking algorithms is important for the following reasons: it affects movement of materials into void regions, and the diffusion of material interfaces during material advection. Therefore, it controls the numerical mixing of materials. This, in turn, influences spatial density distributions and their time-evolution, the effective strength of distributed solids, and so, ultimately, the amount of material ejected and its propagation during impact problems. It is also true that the problem of accurate interface tracking becomes more difficult in 3-D calculations and also more important, given the greater limitation on grid resolution. Ultimately, this type of problem is a *sub-grid resolution* problem, in which information on length scales smaller than the size of a cell is important for accurate computations.

In two-dimensional calculations CTH offers the option of using a high-resolution interface tracking (HRIT) algorithm similar to a method suggested by Youngs [1,8]. The SLIC scheme of Noh and Woodward [9] is also included. The simplest example of the effect of enhanced interface tracking is depicted in Figure 7, where the results of a test problem are shown. Figure 7a shows three objects (two crosses and a figure-eight) resolved by five zones between the interfaces, at $t = 0$. Figure 7b (SLIC) and 7c (HRIT) show these objects after 137 cycles and 139 cycles, respectively, of pure translation at 45 degrees through the uniform mesh. The objects, while they are drastically transformed by the SLIC algorithm, are only slightly modified by the HRIT. In addition, by the time of Figure 7c for the HRIT the objects will not undergo additional change of shape.

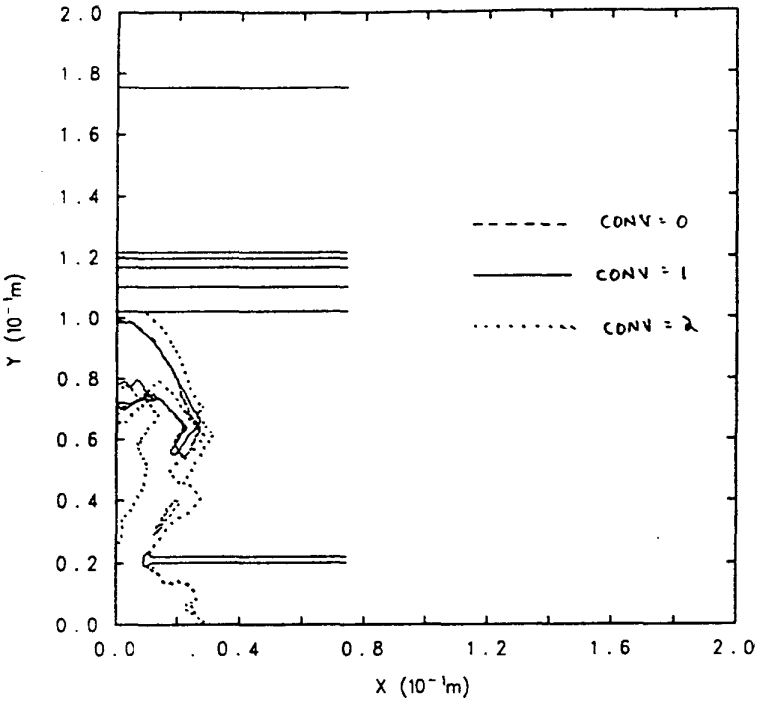

(a)

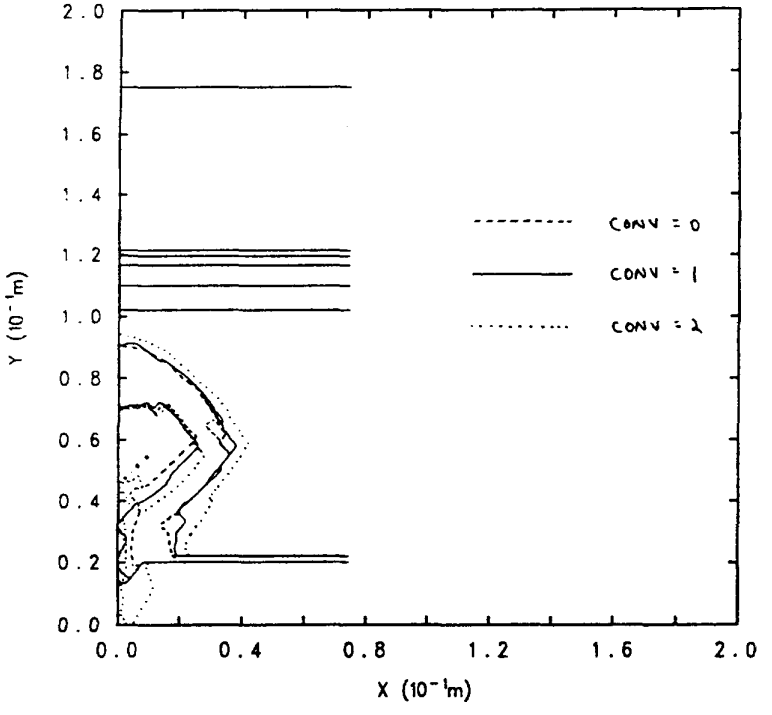

(b)

Figure 5: Material interfaces for (a) v = 7.0 km/s at t = 10.0 μsec and (b) v = 70.0 km/s at t = 0.8 μsec. for the three different advection schemes.

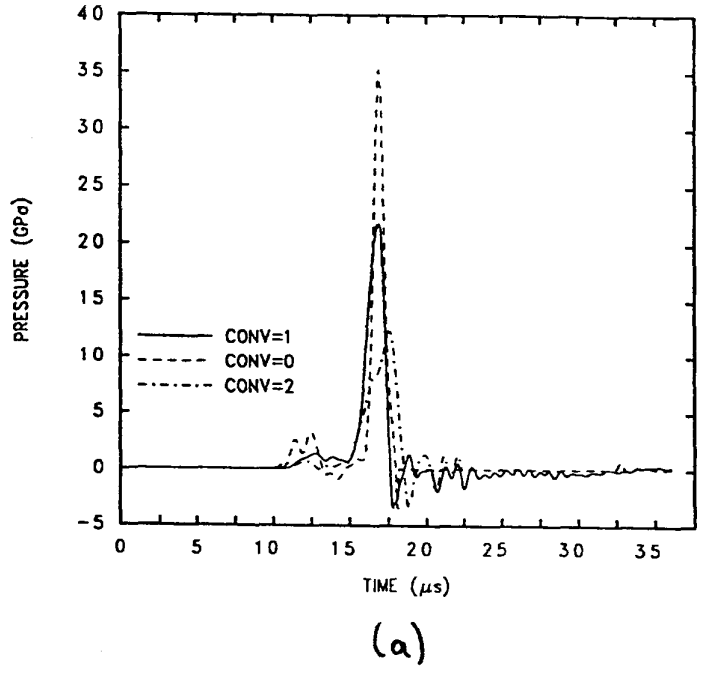

Figure 6: Pressure vs time at location A for three different velocity advection schemes for (a) v = 7.0 km/s and (b) v = 70.0 km/s.

A more practical illustration of the implications of this kind of interface tracking is shown in Figure 8, where we have compared material interfaces from two calculations using SLIC and HRIT for the CP at $v = 70.0$ km/s. The 45° biasing of the SLIC method is prominant in Figure 8. Some "squaring" of the debris cloud occurs with the HRIT. This indicates that more work is needed on the HRIT and its coupling to the other hydrodynamic algorithms. The difference in shapes of the debris clouds is about the same for the $v = 7.0$ km/s case.

The differences in pressure loading at A due to different interface tracking algorithms are again substantial. This is plotted in Figure 9, for both $v = 7.0$ km/s and $v = 70.0$ km/s. For the lower velocity, the peak pressure difference is approximately 50 %. For the higher velocity, the peak pressure difference is only about 10 % at A, but increases with radius. This confirms that interface tracking is most sensitive near the edges of the debris cloud.

2.3 Fragment Motion

McGlaun, *et. al.* [1] discuss a stochastic algorithm implemented in CTH that allows material which lies in a cell surrounded by void to move at statistically correct velocities. This can make a substantial difference in impact problems for which the debris is extremely fragmented. In Figure 10, we show a comparison of the dot density plots of the CP for $v = 7.0$ km/s just prior to stagnation. A certain amount of material is lost from the debris cloud, particularly near the edges, if the fragment moving algorithm is not used. There is very little difference in these plots for the $v = 70.0$ km/s case, as we should expect since there will be very little or no fragmented debris in that case.

In Figure 11, we have plotted the corresponding pressure loading histories at A, for both choices of velocity. The differences are smaller for $v = 70.0$ km/s (about 20 %). This is a larger difference than we might expect from examination of the dot density plots, and illustrates how sensitive the pressure loading histories are to algorithm changes. The differences at the low velocity are quite large (approximately 100 %).

The fragment moving algorithm influences the shape of debris clouds, and particu-

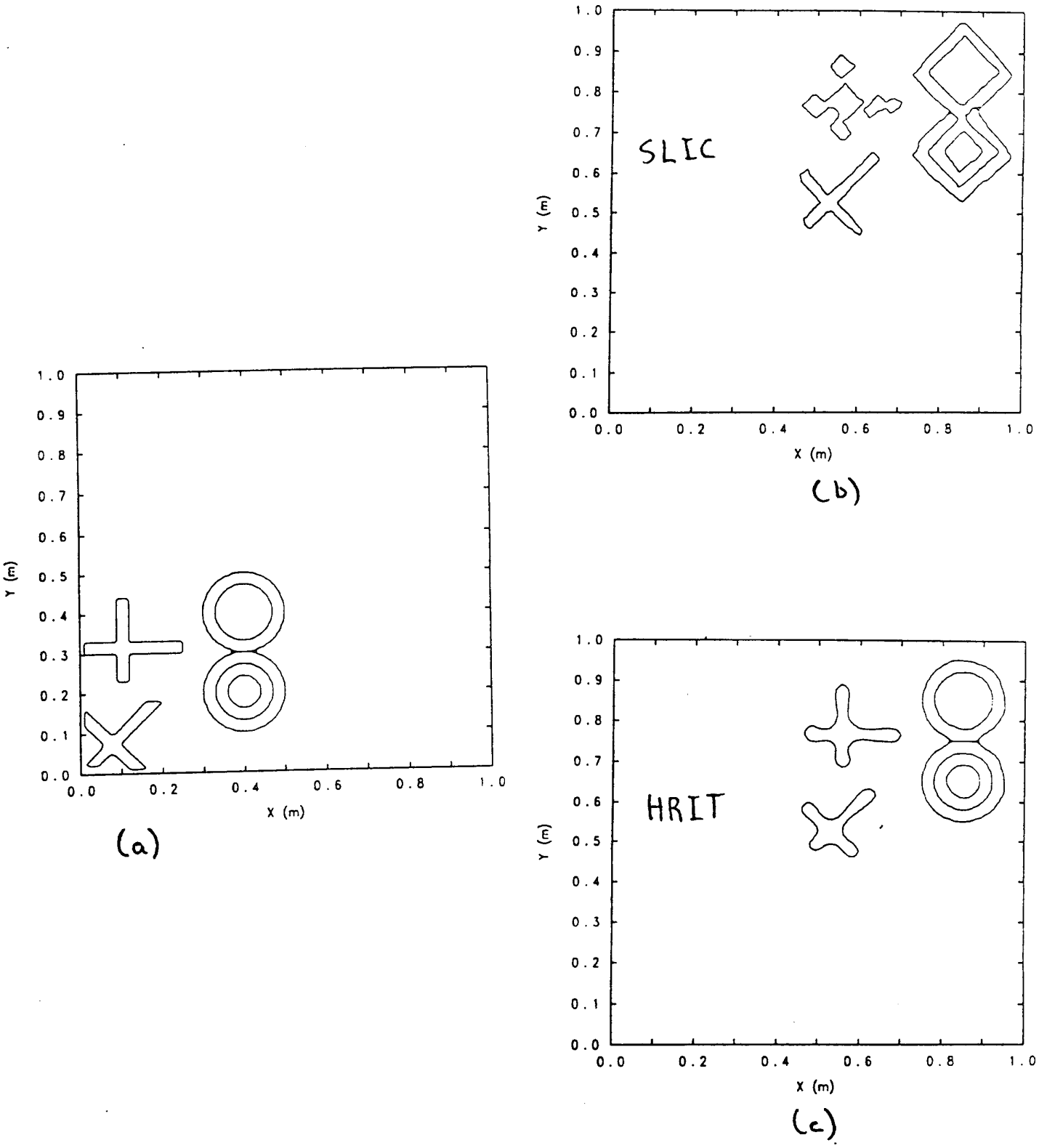

Figure 7: Results of a simple test problem comparing the SLIC and HRIT methods.

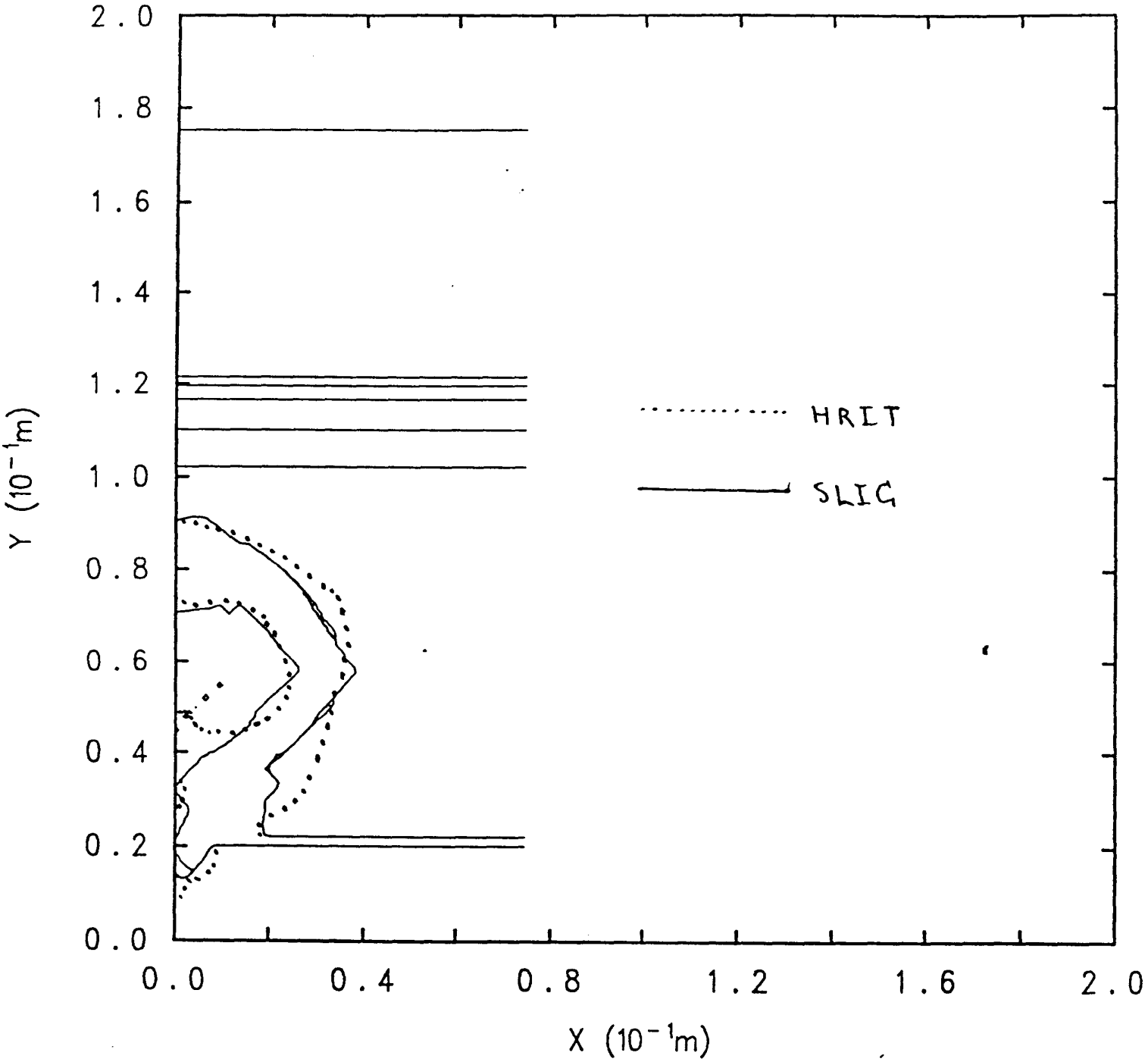

Figure 8: Comparison for the v = 70.0 km/s CP at t = 0.8 μsec between the SLIC and HRIT algorithms.

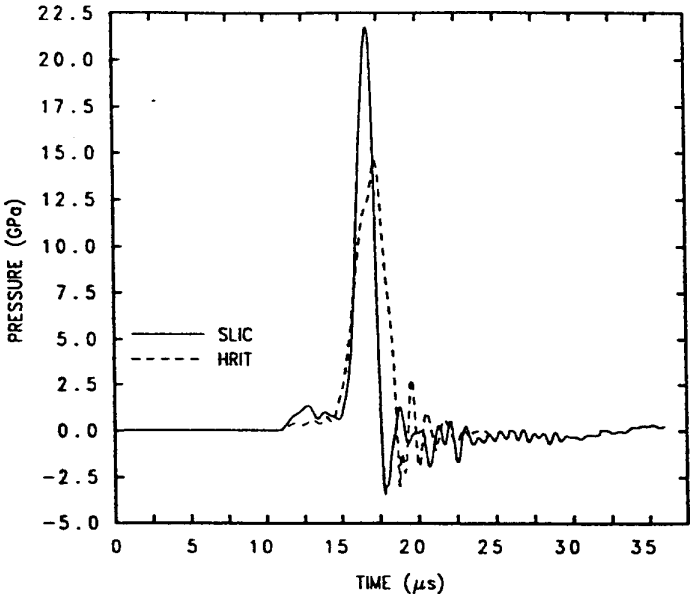

(a)

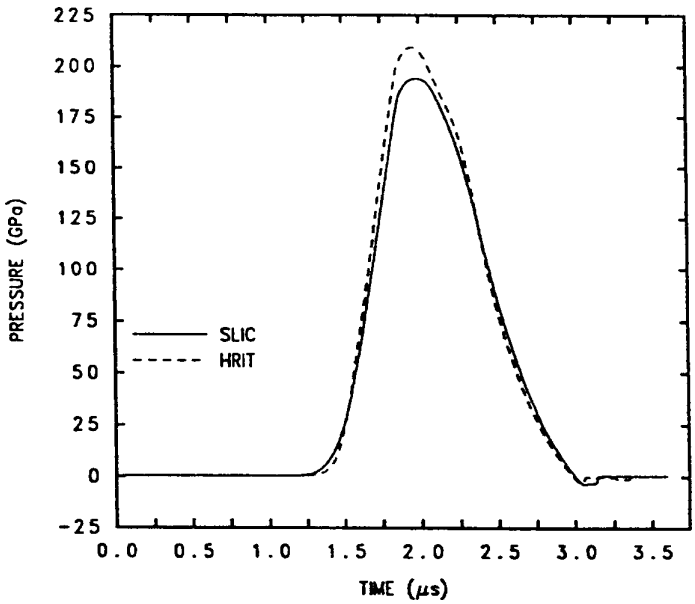

(b)

Figure 9: Pressure vs time at location A for SLIC and HRIT algorithms for (a) v = 7.0 km/s and (b) v = 70.0 km/s.

larly the density distribution of material within them, particularly when large amounts of material fracture occur. The proper fluxing of "gravel" of this type through an Eulerian grid is difficult, properly lying in the domain of sub-grid phenomena and non-continuum mechanics. We do not claim that the fragment moving algorithm is the best resolution of these difficulties. There is clearly a strong link of this issue to proper fragmentation modeling within the hydrocode, a subject that we will not discuss here. The reader can find additional discussion of these points in Trucano, *et. al*, [10].

3 Remarks on Equation of State

We refer the reader to Bjork [11], Holian and Burkett [12], Holian and Holian [3], and Anderson, *et. al.* [2], for a complete discussion of equation-of-state (EOS) issues that are important to the modeling of hypervelocity impact events. These authors have been primarily concerned with the question of how the treatment of vaporization in an EOS can influence the results of hydrodynamic calculations of very high velocity impacts. Asay and Trucano [6] suggest that these issues are not understood for well-controlled experiments in which mixed liquid/vapor debris is created and quantitatively diagnosed. Here, we consider a somewhat different question, namely the sensitivity of simulations to the presence of the melting transition in the EOS.

ANEOS (Thompson and Lauson [13]), the EOS model used in CTH, provides a thermodynamically consistent treatment of the solid/liquid transition, including modeling the latent heat of fusion and the volume change that results from crossing the melt boundary. (Anomalous substances for which the volume decreases upon melting cannot be modeled by ANEOS.) This substantially increases the computational effort required to perform the simulations. For example, More, *et. al.* [14] use a formulation in which the latent heat of melting is ignored. Tabular EOS approaches, for example SESAME, have difficulty providing well-behaved derivatives for the iteration schemes used in the mixed-material cell thermodynamics algorithms in CTH for materials near the triple point.

What are the merits of including this complexity? In Figure 12a we show the pressure at location A with and without the melt transition included for the CP at 7.0

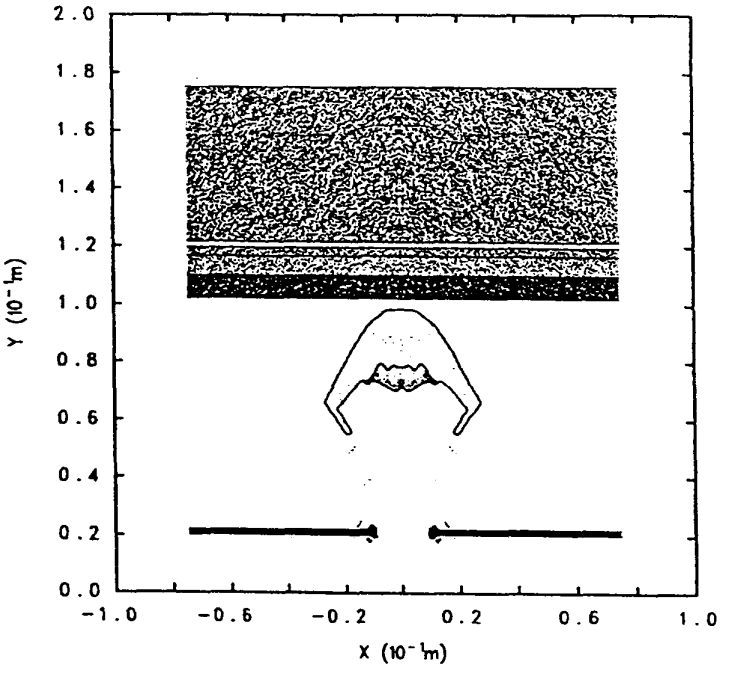

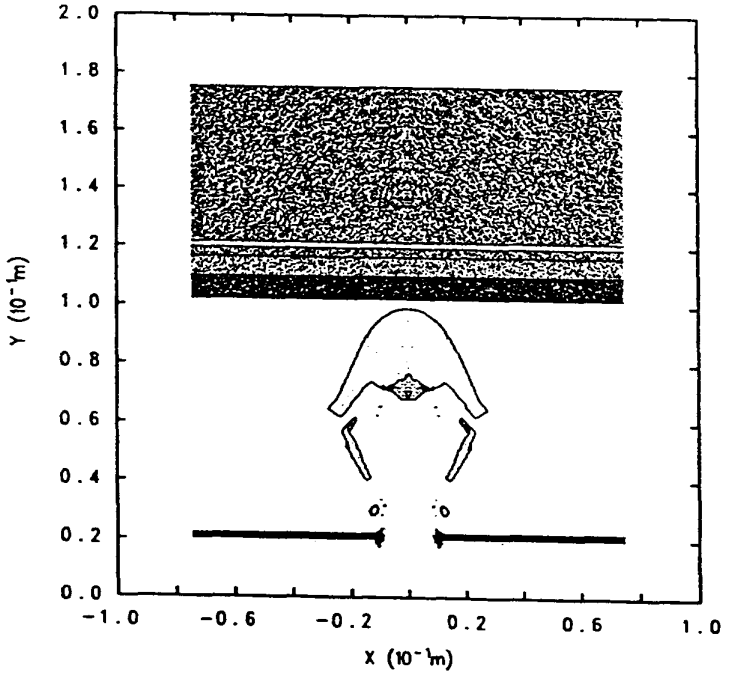

Figure 10: Comparison of dot density plots at t = 10.0 μsec (a) with and (b) without the fragment moving algorithm for v = 7.0 km/s.

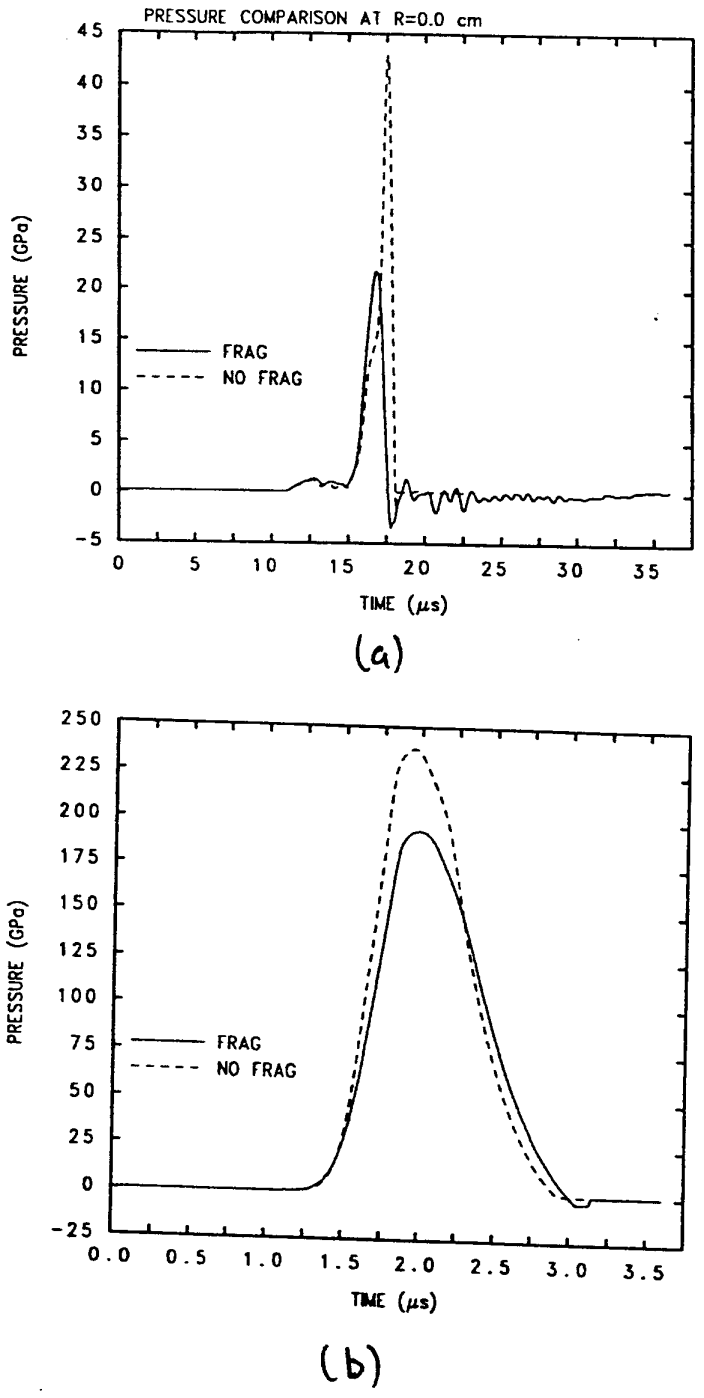

Figure 11: Pressure vs time at location A with and without the fragment moving algorithm for (a) v = 7.0 km/s and (b) v = 70.0 km/s.

km/s impact velocity, while in 12b we show this for a 70 km/s impact velocity. We see that the change in peak pressure is approximately 100 % for the lower velocity. The magnitude of the difference varies irregularly with increasing radius, but it is always large. The error is smaller for the higher velocity case, and becomes smaller at locations with greater radius. This is sensible because there is mainly vapor in the debris cloud. In fact, the differences we are seeing in the higher velocity case are primarily the effect of the melt transition in the secondary target structure, specifically the second layer of tantalum. The real difficulty in dealing with this issue is seen in Figure 13, where we have plotted $\triangle t$ and total CPU (execution) time for both of the impact velocities. The time steps are similar, while the CPU time is 25 to 30 % greater when the melt transition is allowed in the materials. This is a large difference in computational expense for 2-D calculations, and is more so for 3-D calculations. The difference in stagnation pressures for the highest velocities might not warrant the extra expense, while the very large difference for the low velocity impacts seems to demand it. Unfortunately, the lowest velocity calculations also take about 30% longer to compute.

4 3-D Calculations

We emphasize that all of the sensitivities that we have discussed here, and that are discussed in the references, become even more important in three dimensional calculations, primarily because of the greater restriction upon the resolution of the grid. With this in mind, we now illustrate the 3-D capabilities of CTH by presenting the results of a three-dimensional simulation similar to the CP. The simulation models the impact of a tungsten sphere, 0.3125 cm in diameter, normally upon a 0.15 cm thick lead plate at 6.5 km/s. The resulting debris is allowed to stagnate against a target consisting of 0.2 cm of aluminum backed by 1.2 cm of lithium fluoride. This calculation, and its 2-D equivalent, was part of a set of design calculations for a proposed series of terminal ballistics experiments.

Because of the assumption of normal impact, the computations can be performed in an octant of space, defined by:

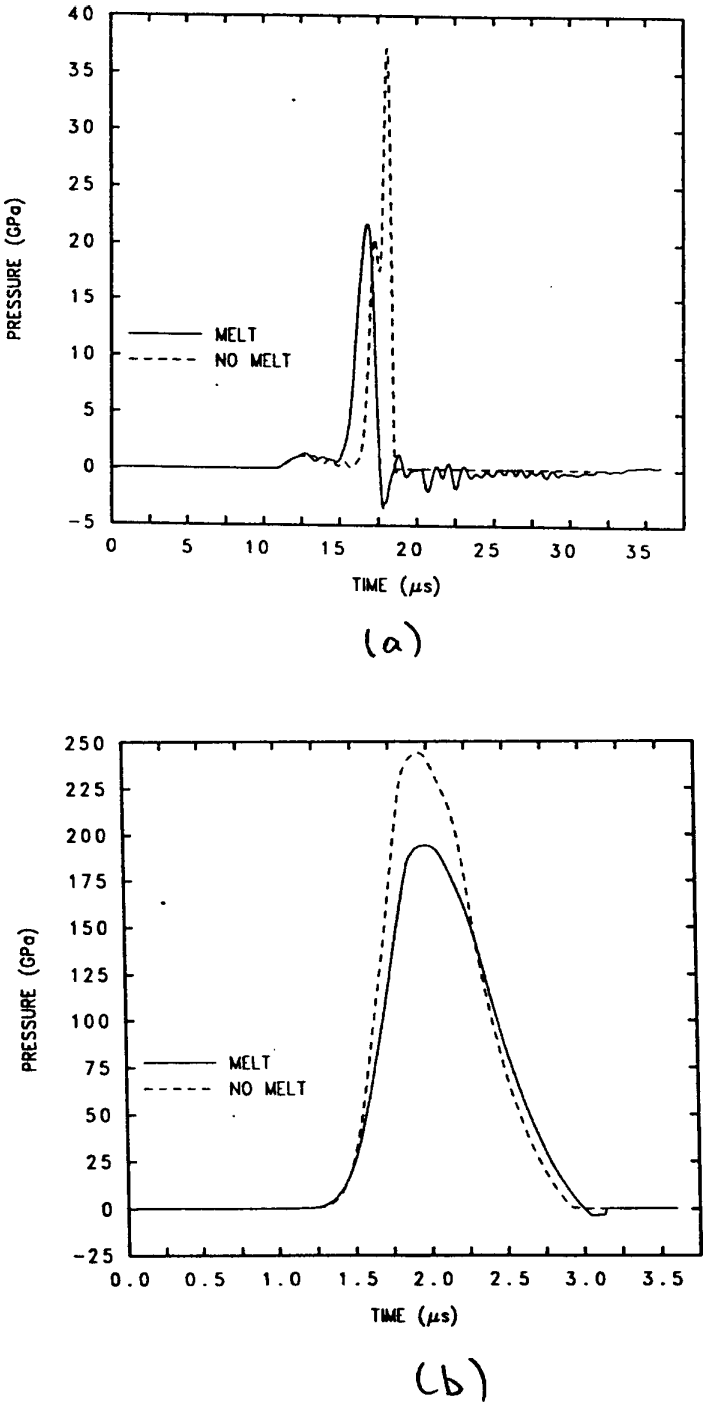

Figure 12: Pressure vs time at location A with and without the melt transition for (a) v = 7.0 km/s and (b) v = 70.0 km/s.

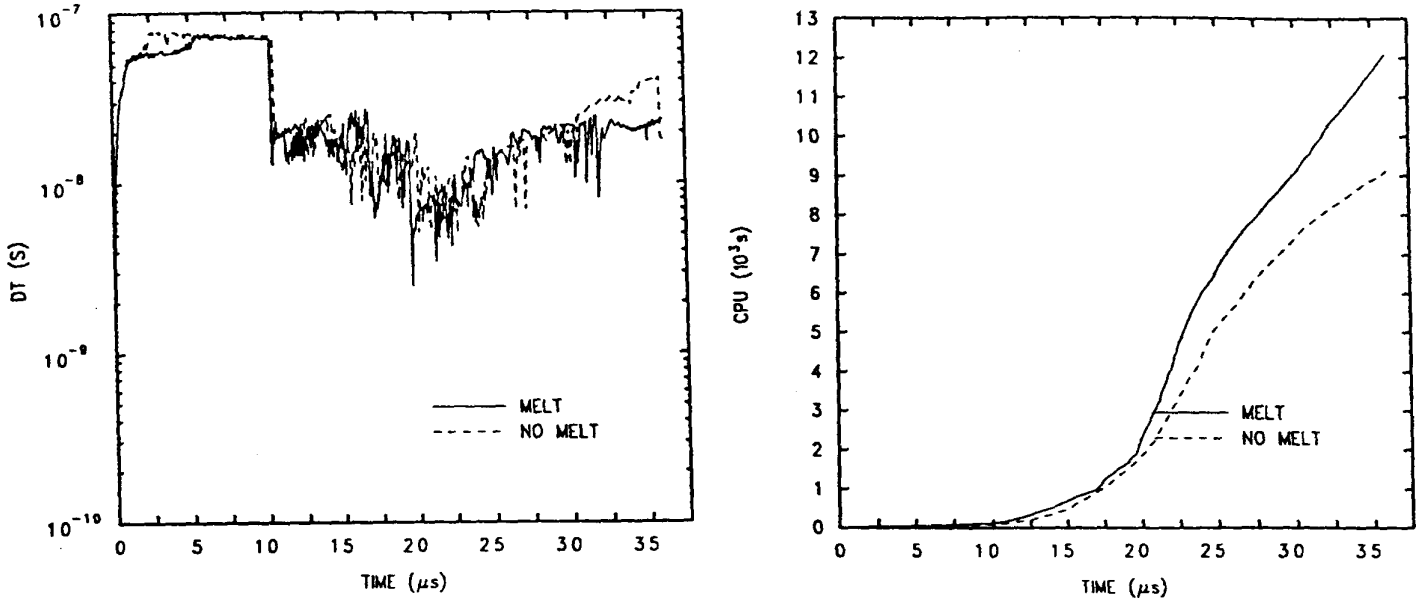

(a)

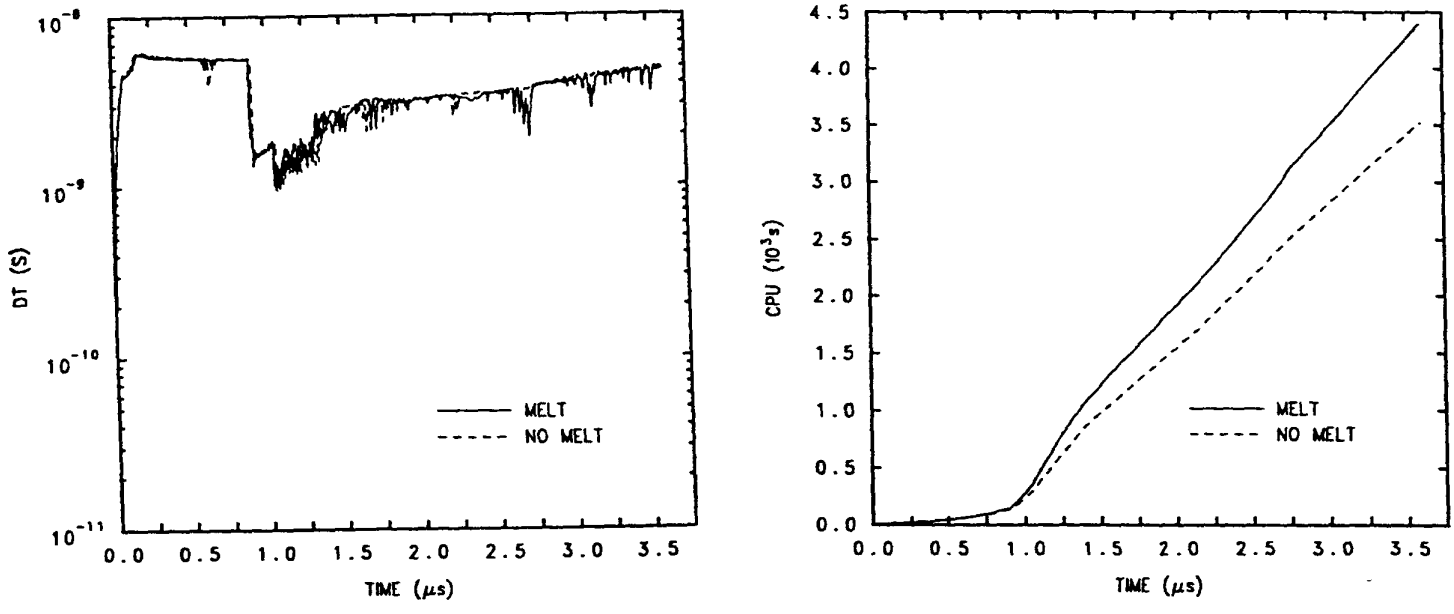

(b)

Figure 13: Δt and CPU versus time with and without the melt transition for (a) v = 7.0 km/s and (b) v = 70.0 km/s.

$$0 \leq x \leq 2.0 \text{ cm}, \qquad N_x = 80$$

$$0 \leq y \leq 2.0 \text{ cm}, \qquad N_y = 80$$

$$-1.0 \leq z \leq 3.05 \text{ cm}, \qquad N_z = 122$$

$$3.05 \leq z \leq 4.35 \text{ rm}, \qquad N_z = 24$$

The number of uniform zones in each direction is given by N_x, N_y, and N_z, with the resolution the same as for the 2-D calculations discussed above. The second value of N_z reflects a set of variable size zones resolving the rear portion of the lithium fluoride. The total number of zones in this problem is therefore 934,000. This requires almost 29 million words of storage on a Cray XMP 416. The Cray Solid State Disk external storage device must be used to execute calculations of this magnitude. The 3-D calculation was run to 3.62 μsec of problem time, which took approximately 15 CPU hours on the XMP 416. Symmetry boundary conditions were applied at the planes $x = 0$ and $y = 0$. The direction of impact is along the z-axis. All the other code options are identical to the calculation presented in Figure 3. The SLIC method must be used for interface tracking in 3-D CTH calculations at this time. The output, in the form of a series of binary dumps of the database, resided in approximately 28 million Cray words. (Database compaction routines in the code reduced it to this size, which represents about 8% of its uncompacted form.)

In Figure 14, we compare interfaces of the 3-D calculation in the $x = 0$ plane and the $y = 0$ plane with the interfaces from the corresponding 2-D calculation at a time shortly before stagnation. We see relatively small differences between the 2-D and 3-D calculations. We also note that the differences between the $x = 0$ plane and $y = 0$ plane are *very* small, but non-zero, reflecting slight asymmetries in the operator split advection routines. Note that the HRIT was used in the 2-D calculation.

As we mentioned above, the comparison of material interfaces can show deceptively small differences between calculations. In Figure 15, we have plotted the comparison of the 2-D and 3-D calculated pressure history at location A. The 2-D calculation was executed to a slightly longer problem time. We see major differences between the calculations. The structure of the 2-D calculation seems to be more complex. We

emphasize that this is not an artifact of zoning differences - the resolution in both calculations was identical. Arrival times are in fair agreement, as is the timing of the peak near 3.3 μsec. However, the 3-D calculation wasn't executed long enough to determine whether the double peak structure seen in the 2-D calculation is preserved.

The initial disturbance is due to the arrival of lead debris (partially vaporized) at the aluminum interface. The second, much larger, disturbance results from the arrival of tungsten debris (solid fragments). At this time we can not explain the large differences between the 2-D and 3-D calculations for this feature. Our earlier discussion of interface tracking does suggest that we may be seeing a result of the differing interface tracking treatments. Originally, we argued that stagnation pressures of tungsten fragments for the CP at impact velocities of 7.0 km/s could vary by about 100 %, depending on the use of SLIC or HRIT. While the differences seen in Figure 15 are even larger, they are not an order of magnitude larger, and interface tracking may be the cause.

5 Conclusion

In this paper, we have illustrated the use of the strong shock wave physics computer program CTH in hypervelocity impact analyses. We have done this by analyzing the sensitivity of computed hypervelocity impact phenomena to some of the algorithms that have been implemented in CTH. The algorithms have all shared the common feature that there exists no "correct" treatment. We also now suggest that, in the absence of sufficiently quantitative experimental data in the velocity regime that is of interest, there may also be no "best" treatment. It is clear from the results that are reported here that approaches which yield relative qualitative agreement of numerical predictions can have large quantitative differences. This means that a greater burden lies on experiments to provide better quantitative data for comparison with numerical simulations. This conclusion is not intended to be restricted to the hypervelocity impact applications discussed here, since the basis for our conclusion is broader than that.

It is clear that grid resolution is a major limitation in hypervelocity impact calculations, even for 2-D calculations. The problem is expecially bad when impact generated debris must be propagated over large distances, to subsequently strike other struc-

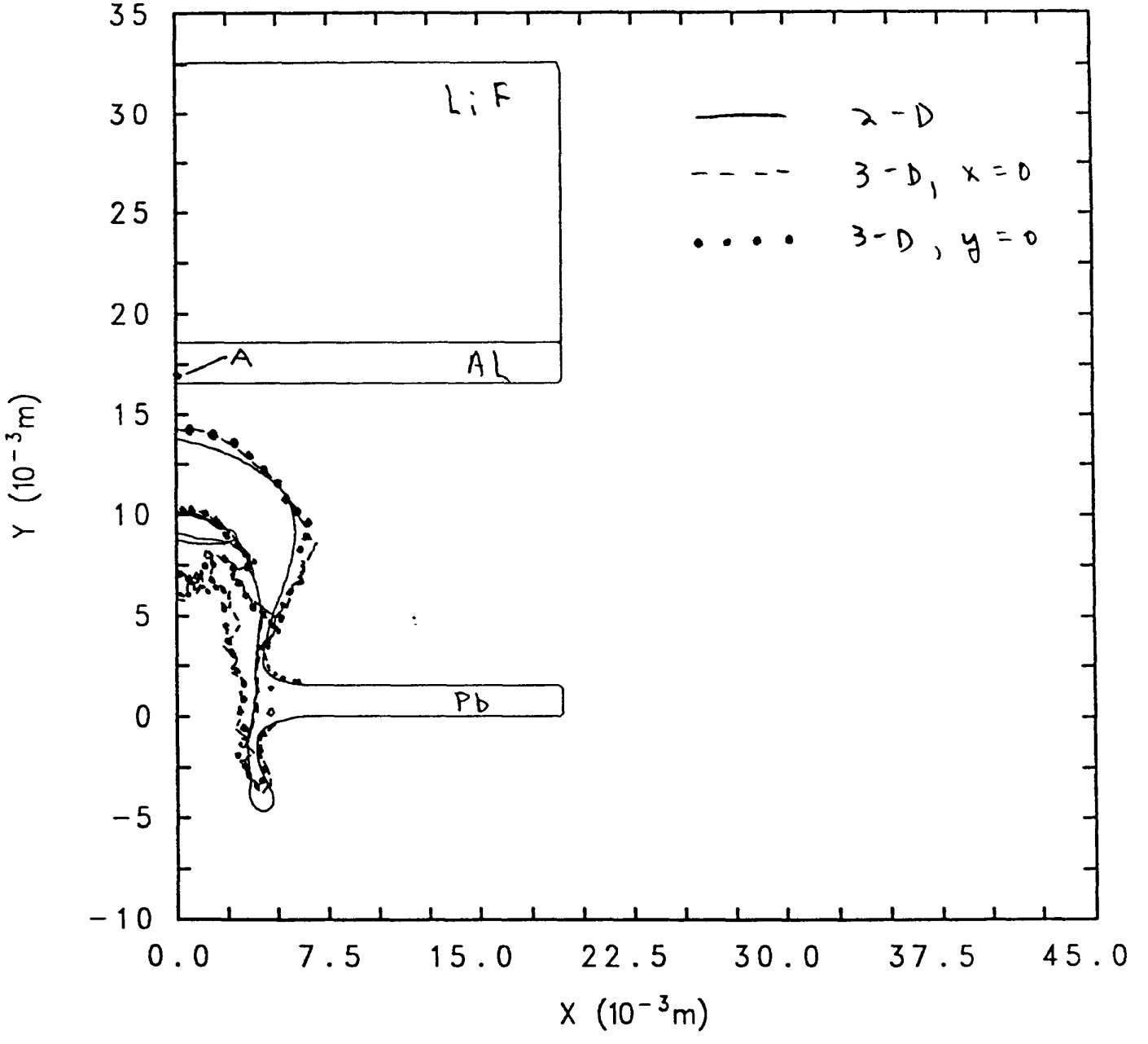

Figure 14: Comparison of material interfaces for a 2-D and two planes of a 3-D calculation.

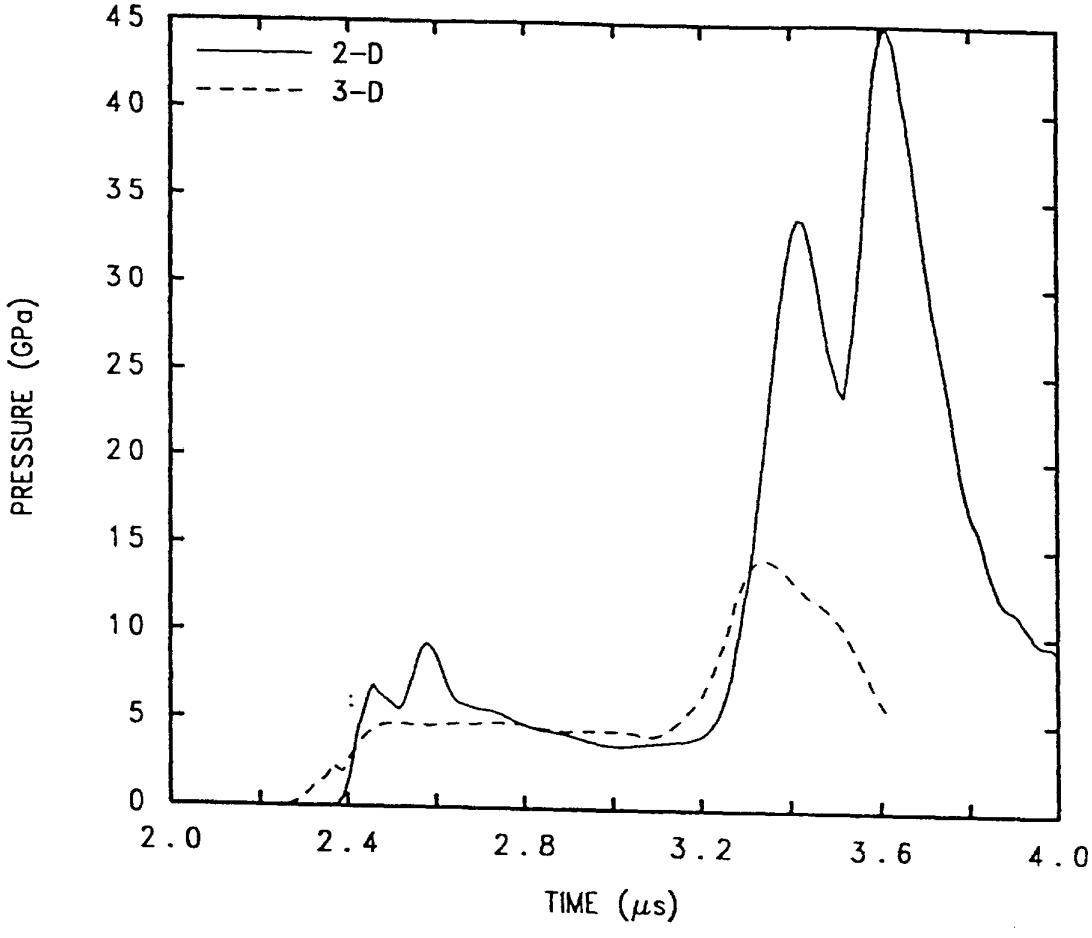

Figure 15: Comparison of pressure loading histories at location A in Figure 14.

tures. The resolution difficulties simply become much greater in 3-D problems. A natural question is how observed large sensitivities related to the failure to simultaneously conserve momentum and kinetic energy during advection (a mathematical fact that we must live with!), to the choice of interface tracking and other sub-grid details of the solution algorithms, and to details of the EOS depend upon the resolution of the calculation. We can not answer this question at the present time. However, we hypothesize that the differences observed due to advection algorithms and sub-grid resolution algorithms will tend to decrease as computational resolution increases. After all, the finite nature of the grid is most directly reflected in algorithms of this kind. EOS issues, on the other hand, will then still remain, as has been pointed out by other authors. For the forseeable future, however, we anticipate that sensitivities like those observed here will continue to be important.

Three-dimensional calculations are currently performed in the field of hypervelocity impact, yet it seems to be true that the current supercomputer hardware environment is not quite capable of handling a large job load of 3-D calculations. We have included an illustration that is a rather *small* illustration of these problems. Problems requiring *hundreds* of hours of computation time are easy to construct. The SSD on the Sandia XMP-416 only holds 256 million words of storage. Problems requiring one billion words or more for sufficient resolution exist and are in need of analysis. Few researchers have access to a modern supercomputer in which they do not compete with other people for machine resources. Not only does this limit the amount of data that can be produced during simulations, but it also influences the amount of wall-clock time it takes to do the work. On a busy machine, a 100 hour job could take one month or longer. Multi-tasking a code such as CTH (which has been done using the Los Alamos National Laboratory Autotasking Library) provides a means of shortening the wall-clock duration by a factor roughly equal to the number of processors on the machine, provided the full resources of the machine can be commandeered. On a crowded multi-processor computer this is not possible, yet significant benefits may still result from running multi-tasked code. This is a future direction of research that will significantly influence our ability to perform 3-D computations as readily as 2-D computations.

References

1. J. M. McGlaun, S. L. Thompson, and M. G. Elrick, CTH: A Three-Dimensional Shock Wave Physics Code, 1989 Hypervelocity Impact Symposium, to be published (1989).

2. C. E. Anderson, Jr., T. G. Trucano, and S. A. Mullin, Debris Cloud Dynamics, Int. J. Impact Engng., to be published (1990).

3. K. S. Holian and B. L. Holian, *Int. J. Impact Engng* **8**, 115 (1989).

4. K. S. Holian, Hydrocode Simulations of Hypervelocity Impacts, in *Shock Waves in Condensed Matter 1987*, edited by S. C. Schmidt and N. C. Holmes, North-Holland (1988).

5. T. G. Trucano, J. R. Asay, and L. C. Chhabildas, Hydrocode Benchmarking of 1-D Shock Vaporization Experiments, in *Shock Waves in Condensed Matter 1987*, edited by S. C. Schmidt and N. C. Holmes, North-Holland (1988).

6. J. R. Asay and T. G. Trucano, Studies of Density Distributions in One-Dimensional Shock-Induced Vapor Clouds, 1989 Hypervelocity Impact Symposium, to be published (1989).

7. D. E. Grady, T. K. Bergstresser, and J. M. Taylor, Impact Fragmentation of Lead and Uranium Plates, Sandia National Laboratories Report SAND84-1545 (1984).

8. D. L. Youngs, Time-Dependent Multimaterial Flow With Large Fluid Distortions, in *Numerical Methods for Fluid Dynamics*, edited by K. W. Morton and M. J. Baines, Academic Press (1982).

9. W. F. Noh and P. Woodward, SLIC (Simple Line INterface Calculation), in *Proceedings of the Fifth International Conference on Numerical Methods in Fluid Dynamics*, edited by A. I. van de Vooren and P. J. Zandbergen, Springer Verlag, (1976).

10. T. G. Trucano, D. E. Grady, and J. M. McGlaun, Fragmentation Statistics From Eulerian Hydrocode Calculations, 1989 Hypervelocity Impact Symposium Proceedings, to be published (1989).

11. R. L. Bjork, *Int. J. Impact Engng.* **5**, 129 (1987).

12. K. S. Holian and M. Burkett, *Int. J. Impact Engng.* **5**, 333 (1987).

13. S. L. Thompson and H. S. Lauson, Improvements in the CHART-D Radiation-Hydrodynamic Code III: Revised Analytic Equations of State, Sandia National Laboratories Report SC-RR-71 0714 (1972).

14. R. M. More, K. H. Warren, D. A .Young, and G. B. Zimmerman, *Phys. Fluids* **31**, 3059 (1988).